

Wendy H. MÜLLER

F.R.S.-FNRS Research Fellow

PhD thesis supervised by Prof. Gauthier EPPE

Mass Spectrometry Laboratory, MolSys Research Unit, Chemistry Department

University of Liège, Allée du Six Août 11, B6c Sart-Tilman,

4000 Liège (Belgium)

wmuller@uliege.be, +32 (0)4 366 3567



A molecular imaging approach combining Raman Spectroscopy and Mass Spectrometry to study biological samples

Abstract

The study of biological samples, like biological tissues or microbial communities, can be very complicated as such kind of samples are in essence extremely complex. This complexity is mainly expressed by the heterogeneity of their molecular microstructure, both in terms of spatial arrangement and chemical composition. Thus, the analysis of biological samples requires analytical techniques able to visualise the distribution of the chemical compounds within the sample at a molecular level and with a high spatial resolution. To this end, the use of molecular imaging techniques is a promising avenue and, in particular, the development of multimodal approaches (that is, combining several complementary techniques to overcome the limitations of the individual ones) has grown interest in the last decade. Here, we show that the combination of Raman spectroscopy and mass spectrometry imaging represents an up-and-coming implementation of multimodal molecular imaging for the study of complex biological samples.

Keywords

Raman Spectroscopy, SERS, Mass Spectrometry, SALDI-MS, Imaging

1. Introduction

Biological samples, such as biological tissues, cells or microbial communities are complicated molecular systems. Indeed, their heterogeneous molecular microstructure turns out to be both chemically and spatially complex. Yet, the investigation of the chemical composition of biological samples, at the molecular level and with spatial information, is of particular interest in various fields. Indeed, visualising the spatial molecular distributions in cells and tissues and associating them with structural or other biochemical features can, for example, give some insights into the biological mechanisms involved in the development of a disease [1], facilitate clinical diagnosis by identifying the regions of pathology [2,3] or enable the engineering of novel biotechnological applications.

Conventional imaging techniques include histology, immunohistochemistry [4] and fluorescence microscopy, which allow the visualisation of the distribution of targeted molecules within the biological samples. Histology and histochemistry are the standard methods, routinely applied to reveal general tissue morphology, cell type, subcellular structure and the presence of endogenous substances that react

with the stains [1]. However, these approaches are only qualitative. Fluorescence microscopy using dyes or quantum dots has also been extensively used to study biochemical processes, especially at the single cell level, as it provides high sensitivity and high contrast images. However, most fluorescent dyes exhibit photobleaching and photodegradation [5] and the band width of fluorescence peaks are usually broad [5], limiting the multiplex detection (i.e. detection of multiple analytes simultaneously). Moreover, both histological and fluorescence approaches lack of specificity at the molecular level [1,6].

1.1. Emergence of molecular imaging techniques

Nowadays, molecular imaging techniques have emerged as a powerful implementation of molecular analytical techniques to investigate and visualise the complex heterogeneity of the chemical composition of various samples [7-10].

To this end, the sample is analysed by a molecular analytical technique able to record the chemical information at different spatial locations (Figure 1). For example, mass spectrometry and vibrational spectroscopy imaging techniques are particularly well adapted to study biological samples. With these techniques, the biological sample is interrogated by a laser that moves along the x and y axes. A spectrum (either a Raman spectrum or a mass spectrum) is obtained at each (x,y) location. Then, the molecular image (also called *2D cartography*) revealing the distribution of the analytes within the sample is reconstructed through data processing (Figure 1). Finally, the reconstructed images allow the identification of structures and the visualisation of molecular changes occurring in precisely defined regions of the sample. This includes the evaluation of the spatial distribution of metabolites produced, for example, during intercellular communication.

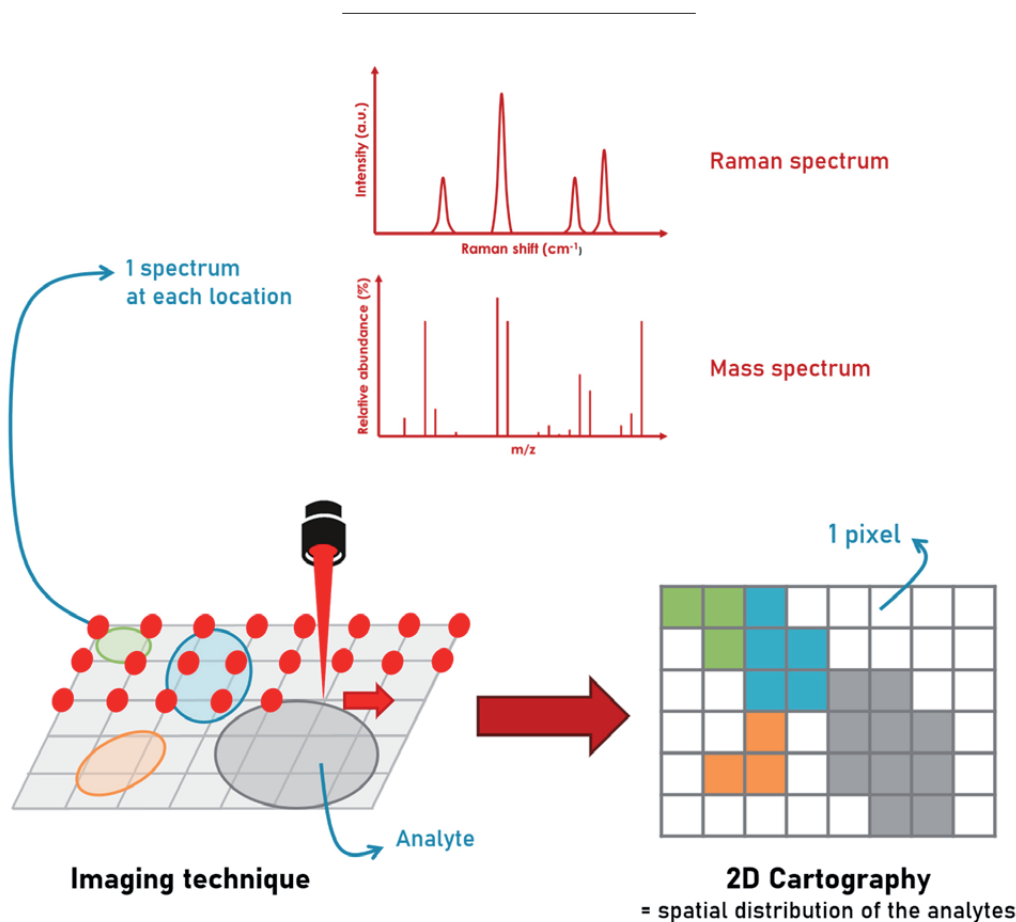


Figure 1: Schematic representation of a molecular imaging approach

2. Molecular analytical techniques to image biological samples

The investigation of the spatial molecular microstructure of biological samples is still a challenge as it requires advanced analytical techniques able to visualise the distribution of the molecular components with both high specificity and high spatial resolution. Multiple imaging modalities can be used depending on the sample and on the desired information [3]. The selection of the most appropriate imaging technique for the sample analysis is not straightforward and depends on several factors such as the required spatial resolution, the levels of sensitivity and specificity, the need for dynamic or *in vivo* information or the need for quantitative information [3]. However, each imaging technique has its own advantages and limitations, therefore a compromise will generally have to be made in order to meet as many criteria as possible. As previously said, there are numerous imaging techniques that can be employed to study biological samples. However, this article will only be focused on Raman Spectroscopy and Mass Spectrometry, which are two complementary techniques commonly used in our laboratory to image biological samples.

2.1. Achieving high spatial resolution with Raman Spectroscopy Imaging

Raman spectroscopy, based on the principle of Raman scattering (inelastic light scattering), is a rapid, non-targeted and non-destructive [11-14] quantitative and qualitative vibrational molecular spectroscopy technique used for the characterisation of either organic or inorganic compounds [8, 15, 16]. During the analysis, a monochromatic light is sent to the sample and the Raman scattered light is then collected and analysed. Raman scattered photons display a shift in frequency, called the *Raman shift*, compared to the frequency of the excitation light [3]. A conventional Raman spectrum (Figure 2) represents the Raman shift on the horizontal axis and the intensity on the vertical axis. In other words, the molecular vibration information can be read on the horizontal axis while the strength

of the activity (intensity) can be read on the vertical axis [17].

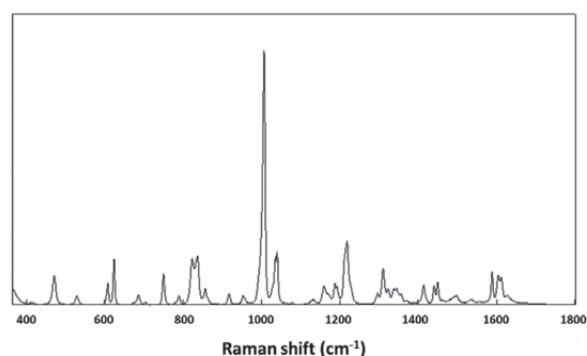


Figure 2: Raman spectrum of Phenylalanine (laser line = 532 nm)

Every molecule has its own unique vibrational signature. Therefore, Raman Spectroscopy can be used to simultaneously detect and identify various molecules within the same area (by deconvoluting or decomposing the complete Raman spectrum into pure components using advanced statistical data treatments) [3].

Raman spectroscopy can also be coupled to optical devices such as microscopes, allowing the imaging of different samples [18] by localising the signals originating from molecular functions, as shown in Figure 3 and Figure 4.

A great advantage of Raman Spectroscopy Imaging is that this technique does not require any specific sample preparation. However, in the case of biological samples, cryosectioning may be necessary to expose the internal section to be imaged. After cryosectioning, sample sections are mounted on a microscopic slide and placed under the Raman microscope to perform the analysis. Some biological samples such as cell cultures in a Petri dish can also be analysed as they are. Sensitive samples might require a chemical fixation step, for conservation purposes, prior to the Raman analysis.

The undeniable strength of this imaging technique lies in the spatial resolution that can be achieved [19] (down to a few hundreds of nanometres), which is requested for the interrogation of biological samples (e.g. mouse brain sections [12, 20]). Spatial resolution in

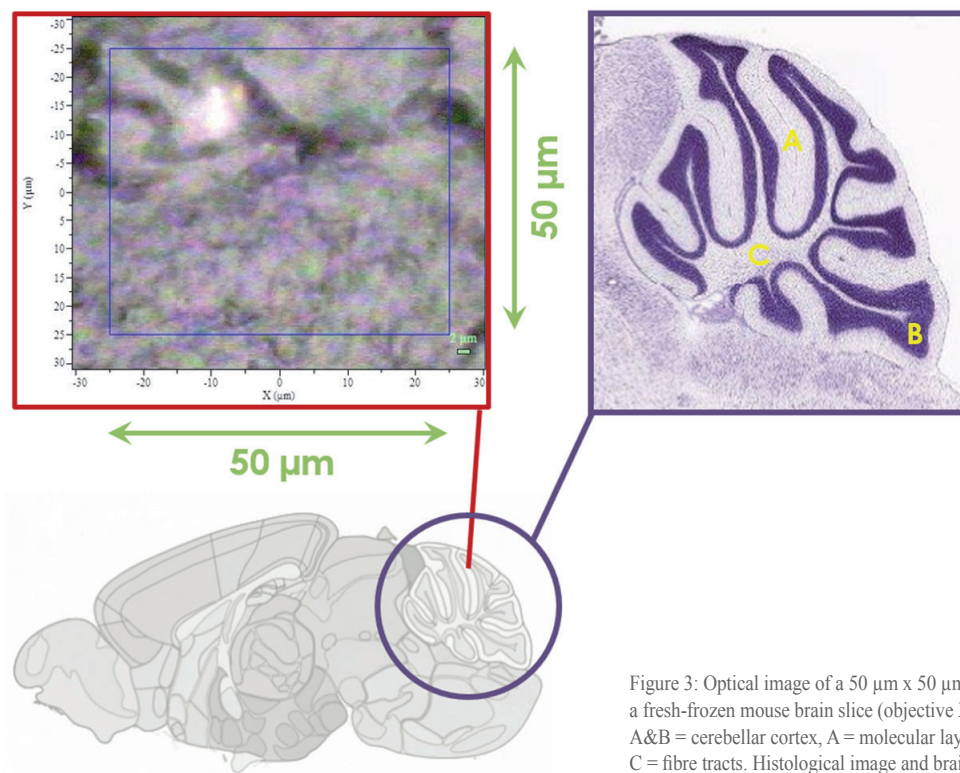


Figure 3: Optical image of a 50 μm x 50 μm area within a fresh-frozen mouse brain slice (objective X50), A&B = cerebellar cortex, A = molecular layer, B = granular layer, C = fibre tracts. Histological image and brain scheme coming from the Allen Brain Atlas [21].

Raman Spectroscopy Imaging is actually only limited by the diffraction limit:

$$R = \frac{1.22\lambda}{2n \sin \theta} = \frac{1.22\lambda}{2NA}$$

With R, the spatial resolution at the limit of diffraction;

λ , the illumination wavelength;

n, the medium refractive index;

θ , half of the angular aperture;

NA, the numerical aperture of the objective.

Because of the relatively short wavelengths used in Raman spectroscopy (UV, visible and near Infrared range of wavelengths) and thanks to the refractive objectives used in Raman Spectroscopy Imaging, micron-scale spatial resolution can be achieved.

Consequently, Raman cartographies can focus on very small regions of interest with a high spatial resolution. As an example, imaging of a 50 μm x 50 μm area of the cerebellum of a mouse brain (Figure 3) was performed by Raman spectroscopy with a spatial resolution of 4 μm. An important part of imaging analyses is the

data processing. Indeed, a significant number of spectra is obtained during the imaging run. It is generally impossible to detect the differences, sometimes subtle, between all recorded spectra without the implementation of advanced statistical data treatment methods. For instance, the 144 pre-processed Raman spectra, recorded in the 50 μm x 50 μm area of the mouse cerebellum, are shown in Figure 4.

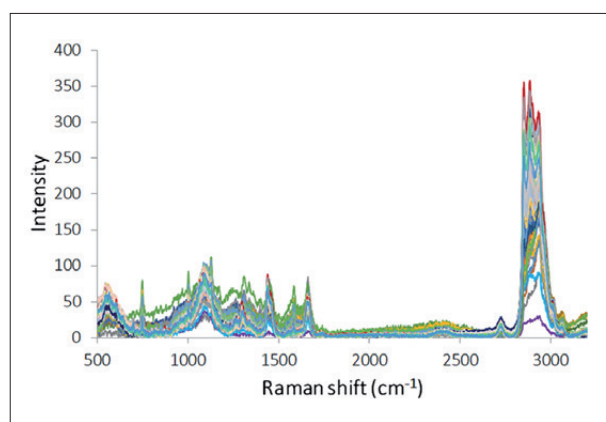


Figure 4: Pre-processed spectra obtained during the imaging of the mouse brain 50 x 50 μm cartography.

In order to identify compounds of interest in the different regions of the cerebellum, Multivariate

Curve Resolution – Alternating Least Squares (MCR-ALS) was used. In a spectroscopic context, MCR-ALS is a data processing method aiming at recovering concentration profiles and “pure” spectra of the corresponding components from an unresolved mixture and therefore, to decompose the signal of the original data into pure individual components. Indeed, MCR-ALS decomposes the complex spectrum in each pixel of an image into a linear combination of pure components spectra (weighted according to their concentration in each pixel). MCR-ALS optimises spectra and concentrations matrices of the pure components of the unresolved mixture under certain constraints. Constraints are criteria of (bio)chemical or mathematical origin that the calculated profiles must fulfil. For example, “non-negativity” constraint has to be applied as both concentrations and band intensity in vibrational spectroscopy cannot be negative.

An MCR-ALS analysis was performed on the dataset comprising all the pre-processed Raman spectra of the mouse cerebellum area. A 3-components model was chosen as, in that case, 3 components are sufficient to explain 99.6% of the total variability of the system. The three pure components spectra are shown on Figure 5 and

images of these pure components distribution within the cartography area are shown in Figure 6.

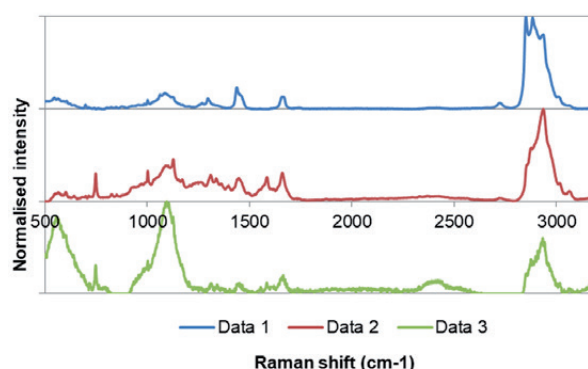


Figure 5: Pure components spectra calculated by MCR-ALS

Assignment of the peaks of the spectra generated by MCR-ALS (**Table 1**) was done and revealed that Data 3 mainly corresponds to the glass spectrum (of the microscopic slide that supports the mouse brain section) with the Raman bands at approximately 560 cm^{-1} and 1100 cm^{-1} , which is why the intensity of this spectrum seems homogeneous within the entire image area (Figure 6). Data 1 is mainly related to lipids. Indeed, the peaks that are only found in the Data 1 spectrum are mainly specific to lipids. On the other hand, Data 2 specific bands indicate an area rich in proteins and nucleic acids and also lipids, which are abundant in the brain.

DATA	Peak value (cm^{-1})	Examples of possible assignment
DATA 1	2884	CH_2 symmetric stretch of lipids, CH_2 asymmetric and CH stretches of lipids and proteins
	2851	CH_2 and CH_3 symmetric stretch of lipids, CH_2 asymmetric stretch of lipids and proteins
	1297	Methylene twisting, fatty acids, CH_2 deformation (lipids), $-(\text{CH}_2)_n-$ in-plane twist vibration (lipid band)
	546	Cholesterol
DATA 2	1585	Phenylalanine $\text{C}=\text{C}$ bending mode, $\text{C}=\text{C}$ olefinic stretch (protein assignment), hydroxyproline
	1361	Tryptophan, guanine
	1172	Tyrosine (protein assignment), (CH) phenylalanine and tyrosine, cytosine, guanine
	748	Thymine (ring breathing mode of DNA/RNA bases), DNA, symmetric breathing of tryptophan (protein assignment)
DATA 3	560	Glass
	1100	Glass

Table 1: Examples of peak assignments of Data 1, 2 and 3 based on widely peak frequencies and assignments of biological tissues [22]

This corroborates with the histological analysis of the tissue since Data 1 corresponds to the white matter rich in myelinated axons and thus rich in lipids, whereas Data 2 corresponds to the grey matter, rich in cell bodies

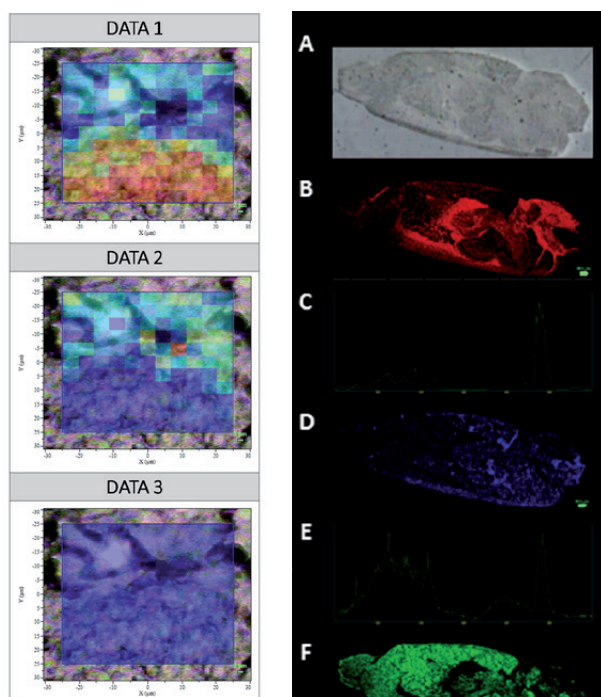


Figure 6: MCR-ALS images showing the distribution of pure components within the area

Figure 7: A-Optical image of a mouse brain section; B, D, F-Raman image of pure components; C, E, G- Raman spectra of pure components; H-Superposition of the three Raman images (C, E & G)

Biological sections can also be imaged on their entire surface. As an example, entire mouse brain sections were interrogated by Raman Spectroscopy Imaging as shown in Figure 7.

As a non-destructive and non-invasive technique, Raman Spectroscopy Imaging can also be performed *in vivo* [14].

However, while Raman spectroscopy does not suffer from water interference, it is deeply impacted by the strong fluorescence signals often emitted by biomolecules or impurities of the sample, which can hide the Raman signals, preventing the acquisition of an interpretable

spectrum [23], as shown in **Figure 8** in the context of bacteria analysis.

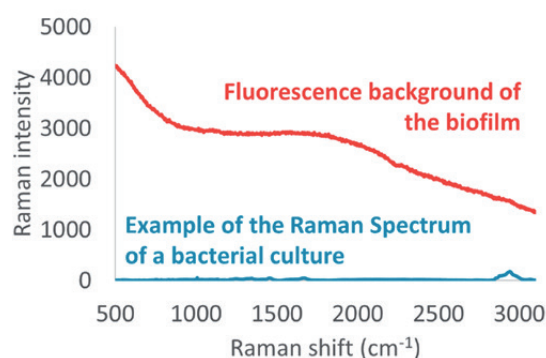


Figure 8: Fluorescence background during acquisition of a Raman spectrum of a bacterial biofilm

Moreover, when light interacts with matter, the Raman scattering is the minor process. Indeed, most photons are elastically scattered (Rayleigh scattering), while only one Raman photon is scattered for $10^6 - 10^8$ Rayleigh photons [3, 24]. Therefore, Raman spectroscopy also suffers from poor sensitivity [19].

2.2. Surface-Enhanced Raman Spectroscopy to improve the sensitivity

However, these drawbacks of Raman spectroscopy (i.e. poor sensitivity and autofluorescence of the samples) can be overcome by the deposition of metallic nanoparticles on the sample surface. Indeed, in this approach, called *Surface-Enhanced Raman Spectroscopy* (SERS), the Raman effect is amplified by 6 to 10 orders of magnitude [25-28] due to the presence of the nanoparticle metallic surface onto which the Raman active molecules are adsorbed (Figure 9).

In opposition to classical Raman Spectroscopy Imaging that necessitates no specific sample preparation, SERS imaging requires the deposition of nanoparticles on the sample surface. To this end, the nanoparticles are suspended in a polar solvent (e.g. water, acetonitrile, methanol, ethanol or a mixture of some of these solvents) and then sprayed onto the sample surface. In our laboratory, the deposition is performed using an automated spotting device, initially developed for the deposition of MALDI matrices, for Mass Spectrometry Imaging, *see MALDI-MS section*)

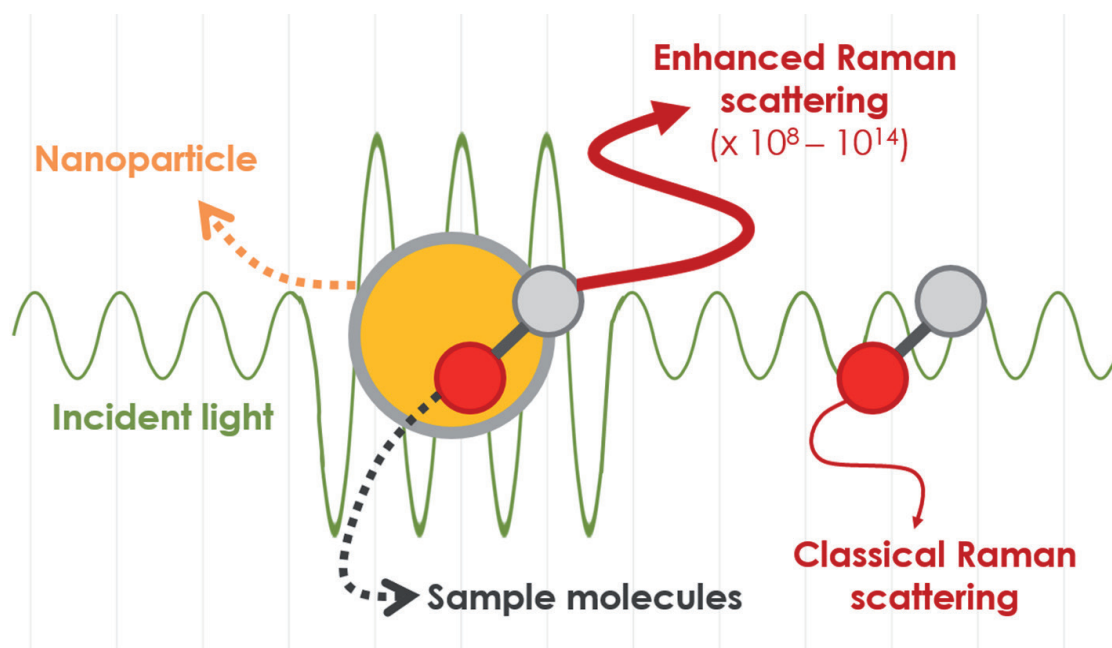


Figure 9: Schematic representation of Surface-Enhanced Raman Scattering

that is equipped with a capillary spray head ensuring the deposition of a homogeneous film of nanoparticles suspension over the sample.

SERS is also based on the principle of Raman scattering and has therefore the same overall advantages and limitations as “classical” Raman spectroscopy. The main difference obviously lies in the signal exaltation in SERS, giving this technique much more sensitivity than “classical” Raman spectroscopy, what can lead to faster image acquisition [19].

The exact mechanisms behind the signal exaltation in SERS are still not fully understood. However, two exaltation paths are generally accepted in the literature: the electromagnetic exaltation and the chemical exaltation [24, 29, 30]. Briefly, the electromagnetic exaltation mechanism contributes to the strongest signal amplification (factor $10^4 - 10^7$) [29, 31] and is due to the excitation of the surface plasmon (shown in Figure 9), which corresponds to a collective oscillation of the conduction electrons of the metal nanostructure [30]. Under certain irradiation conditions, the surface plasmon is activated by the incident electromagnetic radiation (resonant interaction), which increases the electromagnetic field intensity at the close vicinity of the surface of the nanoparticle [29, 32]. In turn, the interaction between this

amplified electromagnetic field and the adsorbed Raman active molecule increases the intensity of the Raman scattering [32]. On the other hand, the chemical exaltation only contributing to a signal amplification by a factor 10^2 has been introduced to explain why different molecules have different exaltation factors in identical experimental conditions [29, 30]. However, this exaltation mechanism is still subject to controversy. Different theories try to explain this exaltation in which the Raman active molecule, chemically adsorbed on a metal, has new resonance “paths”. These resonance paths can be created by the formation of a complex between the molecule and the metal or by the creation of charge transfer complexes between the molecule and the metal [33].

Moreover, metal nanoparticles can quench autofluorescence that is common with biological samples [19, 34].

However, SERS has specific limitations: the signal intensity is not necessarily directly proportional to the concentration of the analytes [35] and suffers from poor reproducibility [19]. Indeed, the signal strongly depends on the nanometric substrate (influence of size, shape and chemical nature, for example) [29]. Moreover, while Raman spectroscopy is considered as a non-destructive

technique, the application of nanoparticles to the sample in SERS may be problematic if other analyses (e.g. histological analyses) need to be later performed on the same sample. *In vivo* applications of SERS are also limited as the potential toxicity of the nanoparticles is still not completely understood.

Unlike classical Raman spectroscopy, SERS imaging can be performed following two different approaches: non-targeted (similar to classical Raman spectroscopy with surface-enhanced signals) and targeted by the use of SERS nanoprobes (Figure 10). The SERS nanoprobes can be prepared from metallic nanoparticles, for example, functionalised with a Raman reporter (a molecule selected to give an intense Raman signal and enabling the detection of the nanoprobe) and a targeting agent, which can be a peptide or an antibody, for instance, specific to a biological receptor or a particular molecule to target in the sample [36].

This targeting SERS approach also allows multi-analyte analyses through the specific molecular spectral signature of different Raman reporters

and the very small peak width of the Raman spectral bands (10 to 100 times narrower than fluorescence peaks) [37, 38], offering SERS promising multiplexing capabilities [3]. In addition, unlike fluorescence, dyes used in SERS are not subject to photobleaching [14, 27].

However, both Raman spectroscopy and SERS have relatively low chemical specificity as they only identify functional groups based on the bonds vibrations. Therefore, in complex biological samples, these techniques will not be able to assign band values to a specific molecule present in the sample.

2.3. MALDI-MS provides a high molecular specificity but suffers from limited spatial resolution

Compared to vibrational spectroscopy imaging techniques, Mass Spectrometry Imaging (MSI) allows the identification of specific ions based on their mass-to-charge ratios and enables their localisation within the biological samples, but with a lower spatial resolution.

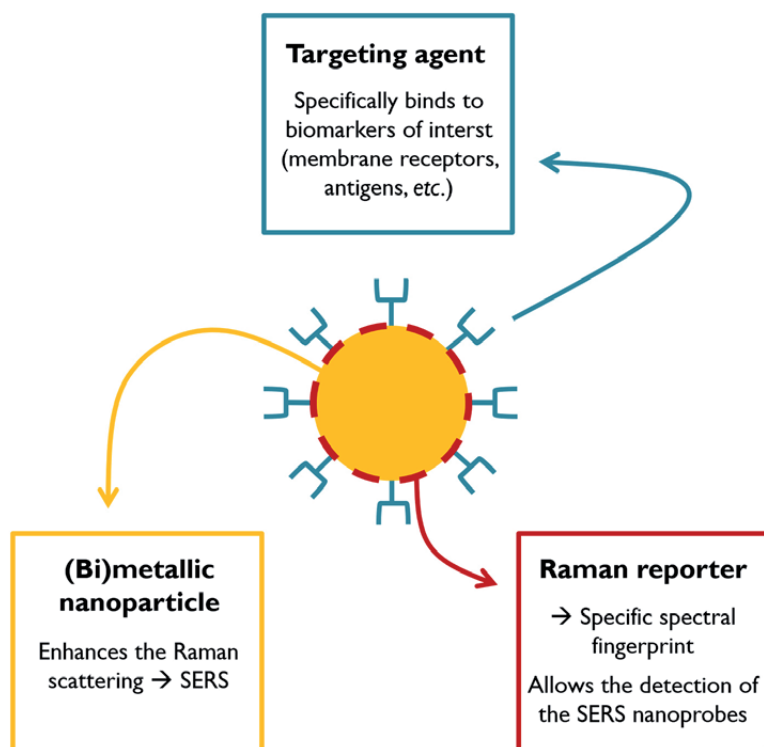


Figure 10: Schematic representation of a SERS nanoprobe

Among the range of ion sources used in mass spectrometry, the soft Matrix-Assisted Laser Desorption/Ionisation Mass Spectrometry (MALDI-MS), which involves a laser striking the sample co-crystallised with an organic matrix in order to promote desorption and ionisation of the analytes, has been extensively used for the imaging analysis of biological samples [10] (Figure 11).

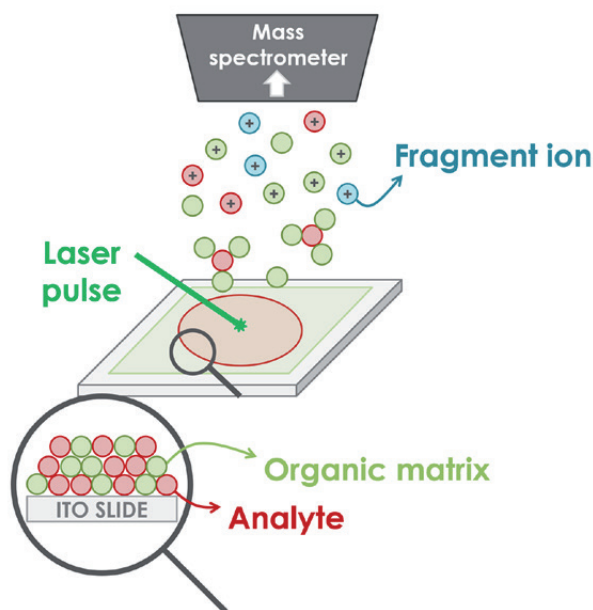


Figure 11: Schematic view of MALDI-MS process

Indeed, MALDI-MS allows the sensitive and rapid analysis of a wide range of compounds [39 - 41], mainly macromolecules (> 700 Da) [42, 43] such as proteins, peptides, lipids and bio-polymers [44] thanks to the formation of monocharged pseudomolecular species ($[M+H]^+$, $[M-H]^-$ and alkali cationised molecules) and limited fragmentation [41, 45]. Moreover, MALDI (and LDI ion sources, in general) are routinely coupled to high resolution mass spectrometry and provide access to the exact and accurate masses of the pseudomolecular ions produced at the surface of the sample [46], providing unambiguous identification of molecules.

Unfortunately, this technique has also several disadvantages, mainly due to the application of the organic matrix chosen to absorb the laser pulse and promote the charge transfer to the sample molecules.

Indeed, the matrix can contribute to ion suppression and spectral interferences in the low mass-to-charge range [2], which often prevents the detection of small molecules and metabolites especially in the range below 700 Da [40, 42, 44, 47-49]. In addition, the organic matrices are also characterised by a lack of reproducibility due to the inhomogeneous co-crystallisation with the analytes [44, 48]. The crystallisation of the matrix is also at the centre of another crucial issue regarding the spatial resolution. Indeed, the spatial resolution obtained with MALDI Mass Spectrometry Imaging (MALDI-MSI) is limited to a few tens of microns, corresponding to the size of the matrix crystals [49] (the crystal sizes of the commonly used 2,5-dihydroxybenzoic acid (DHB) and α -cyano-4-hydroxycinnamic acid (CHCA) are generally comprised between 5 and 20 μm using spraying deposition) [49]. Such resolution prevents to extend the application of MALDI-MS imaging to cellular and subcellular analyses [49].

The sample preparation in MALDI-MSI is also more labour-intensive than in Raman Spectroscopy or SERS imaging). Indeed, the application of the organic matrix applied on the sample with the automated spotting device has to be done carefully in order to ensure an appropriate co-crystallisation of the analyte and the matrix. Moreover, the sample (bacterial culture, tissue sections, etc.) have to be mounted on a conductive support to allow the collection of the extracted ions towards the mass spectrometer.

2.4. From MALDI-MS to SALDI-MS to get around matrix-related issues

Here again, nanoparticles can be used to overcome the limitations of the “classical” well-known technique. Indeed, contrasting with MALDI-MS, Surface-Assisted Laser Desorption/Ionisation Mass Spectrometry (SALDI-MS) employs nanostructured substrates (that may be carbon-based, semiconducting or metallic) instead of organic matrices to promote desorption and ionisation [40] (Figure 12).

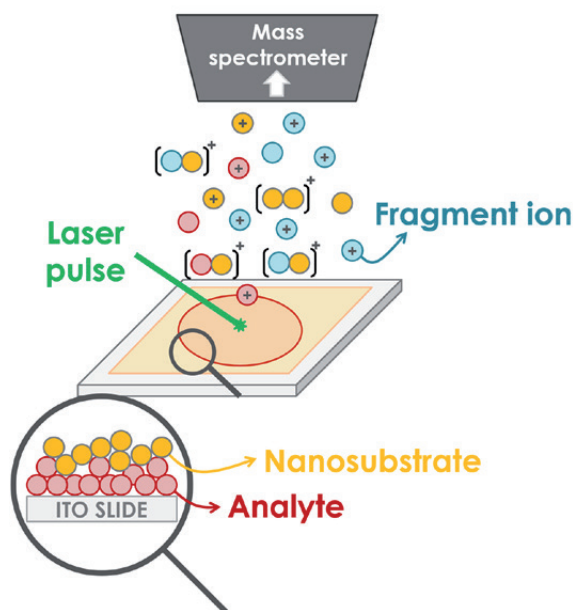


Figure 12: Schematic view of the SALDI-MS process

The SALDI nanosubstrates have the same overall role as the organic matrices: they must be able to absorb the energy of the laser radiation, transfer this energy to the analytes to promote their desorption and provide a source of ionisation [40, 41]. Also, like MALDI-MS, SALDI-MS can be coupled to high resolution mass spectrometry.

In fact, SALDI-MS represents an interesting alternative to MALDI-MS as the use of nanostructured substrates allows to get around the matrix-related issues encountered in MALDI-MS [41, 45].

First, SALDI-MS is particularly effective for the analysis of small molecules (< 1000 Da) with moderate interferences [49, 50], which makes its analysable m/z range complementary to the one of MALDI-MS.

The second interesting feature of SALDI Mass Spectrometry Imaging (SALDI-MSI) is that images can be recorded in both ion modes with the same nanosubstrates (as shown in Figure 14 and Figure 15), while the ion mode in MALDI-MS is generally determined by the choice of the organic matrix. To construct these SALDI images (also called *ion maps*), a peak of the SALDI-MSI mean spectrum (corresponding to a defined m/z value and therefore, to a specific

ion) (Figure 13) is selected and the intensity of this peak in each pixel of the image is represented by a colour gradient to build the SALDI image. The ion map thus shows the distribution of a specific ion in the sample.

Finally, the deposition of nanostructured substrates (following the same procedure as in SERS imaging) instead of an organic matrix eliminates the formation of large matrix crystals, providing visually better images with increasing spatial resolution [49], as shown in Figure 16.

The lateral resolution in SALDI-MSI is indeed only limited by the ionisation laser spot size (which can go down to $5 \mu\text{m}$) and not by the size of the SALDI substrates themselves (as they are nanometric in size) [49, 51].

However, although the improved performances obtained with nanostructured substrates in SALDI-MSI have been increasingly recognised, SALDI-MSI is not used as much as the traditional MALDI-MSI [49]. One reason that could explain this fact is that SALDI-MS involves a series of complicated processes [50, 52], not yet fully understood, which can, in addition, be affected by various physicochemical properties of the SALDI nanosubstrates [44, 50, 53, 54]. Until now, research in SALDI-MS has focused on the engineering of novel substrates with improved performances or on the development of advanced applications in various fields [44]. Only a few studies have focused on the fundamental aspects of the desorption and ionisation mechanisms of the SALDI processes, which is still a subject of much controversy within the SALDI research field.

2.5. Multimodal molecular imaging approaches

As we have just seen in the previous sections, each imaging technique has its own strengths and weaknesses. However, these different imaging modalities should not be seen as competitive as they provide distinct and complementary information about the interrogated samples.

Therefore, in order to maximise the molecular information and to overcome the limitations

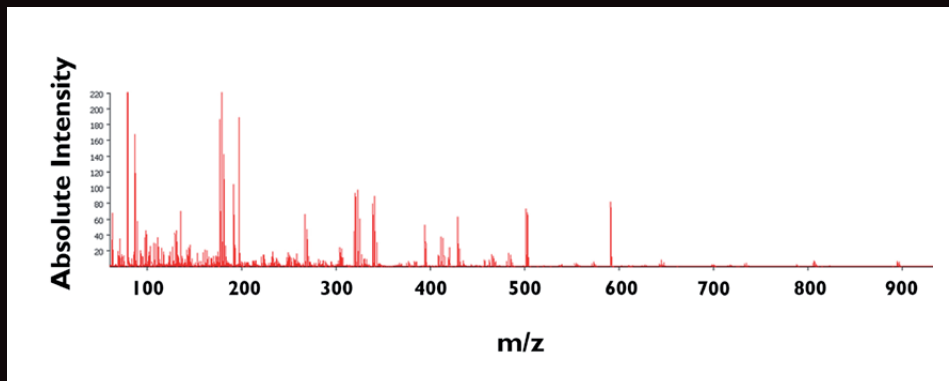


Figure 13: SALDI-MS mean spectrum of the imaging of a mouse brain section in negative ion mode

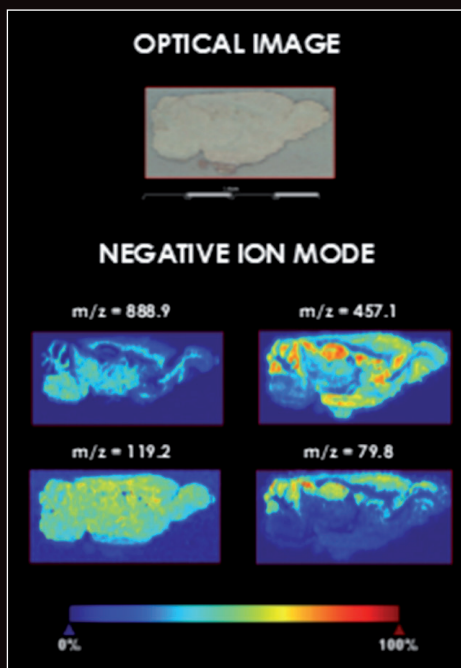


Figure 14: Some SALDI-MS images of the mouse brain section in negative ion mode using bimetallic core-shell gold@silver nanoparticles

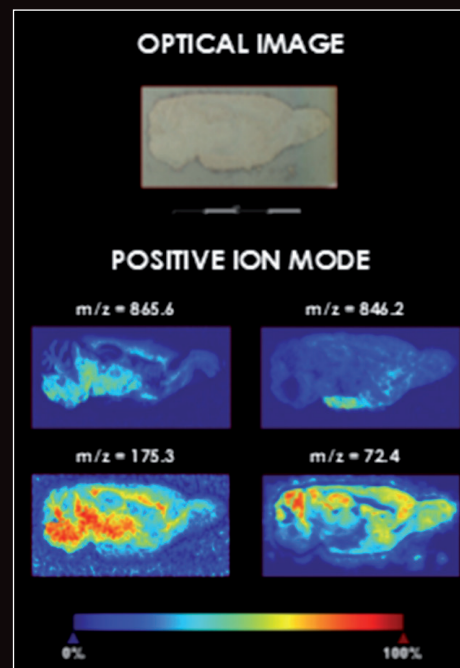


Figure 15: Some SALDI-MS images of the mouse brain section in positive ion mode using bimetallic core-shell gold@silver nanoparticles

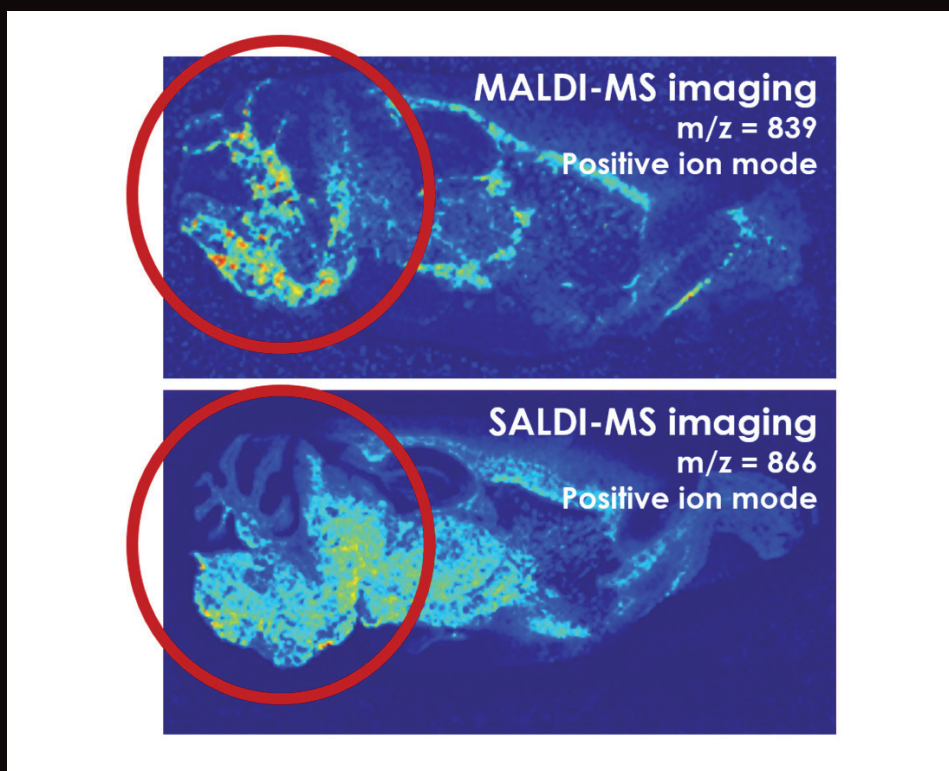


Figure 16: MALDI-MS and SALDI-MS imaging of a mouse brain section in positive ion mode, showing the increased image resolution in SALDI-MS compared to MALDI-MS, with the same laser spot size (i.e. 40 μm)

inherent to each individual technique used separately, several complementary imaging techniques can be combined in a multimodal approach.

A multimodal molecular imaging strategy involving both SERS and SALDI-MS imaging can be implemented on the same biological sample as they both use nanoparticles. This combination is particularly relevant as it benefits from the high spatial resolution of SERS and the high specificity of SALDI-MS imaging. SERS imaging, being a non-destructive technique, can be used upstream of SALDI-MS imaging.

However, if the combination of these two techniques into an integrated multimodal analytical strategy for molecular imaging looks easy on paper, in practice, it turns out to be challenging [19]. For instance, some challenges are inherent to the experimental preparation of the sample that has to be compatible with all the combined techniques [55]. Another challenge concerns the correlation of the molecular images independently obtained by different analytical methods, and thus with dissimilar spatial resolutions (in the (x,y) plane) but also different depths of penetration (z axis). Specific chemometrics statistical tools considering the specificity of all combined techniques as well as the spatial alignment of the images acquired on separate instruments must therefore be implemented [55].

3. Concluding remarks and future prospects

Molecular imaging has the great potential to highlight the spatial distribution of the molecular components in biological samples. It thus enables to reveal the heterogeneous molecular microstructure of tissues, to probe the metabolites excreted during intercellular interactions or to visualise the molecular changes occurring in specific regions of the sample, giving evidence of a pathology.

Various molecular imaging techniques have been developed in the last decades, each individual

technique providing a particular molecular information such as the functional groups present in the molecules or the masses of these molecules distributed within the interrogated sample.

However, these molecular imaging techniques have their own strengths and weaknesses and thus, do not fulfil all the criteria required for an optimal imaging analysis when they are used separately.

That is why the development of multimodal molecular imaging approaches, combining several complementary techniques to overcome the limitations of the individual ones, has grown interest in the last decade. In particular, the combination of SERS and SALDI-MS imaging represents a promising avenue for the analysis of complex biological samples as it reveals the microstructure of the sample at the molecular level, with a high spatial resolution and high specificity.

Some challenges are undoubtedly inherent to the multimodal imaging approaches, such as the sample preparation that needs to be suitable with the combined techniques or the correlation of the molecular images independently obtained with different analytical modalities. Further analytical developments as well as advanced data processing methods are therefore required. Nevertheless, multimodal imaging has already evolved in recent years, opening new opportunities for the study of intricate biological samples. The combination of several molecular analytical techniques offers great potential to address the challenges faced in analytical chemistry applied to biology, biomedicine or biotechnology. We are thus convinced that multimodal molecular imaging approaches will continue to develop in the next five years as the information obtained from multimodal analyses can go beyond what we can learn from the analyses performed with individual techniques.

References

- [1] Bishop, D. P.; Cole, N.; Zhang, T.; Doble, P. A.; Hare, D. J. *Chem. Soc. Rev.* **2018**, *47*, 3770–3787.
- [2] Stopka, S. A.; Rong, C.; Korte, A. R.; Yadavilli, S.; Nazarian, J.; Razunguzwa, T. T.; Morris, N. J.; Vertes, A. *Angew. Chemie - Int. Ed.* **2016**, *55*, 4482–4486.
- [3] James, M. L.; Gambhir, S. S. *Physiol. Rev.* **2012**, *92*, 897–965.
- [4] Zhou, D.; Guo, S.; Zhang, M.; Liu, Y.; Chen, T.; Li, Z. *Anal. Chim. Acta* **2017**, *962*, 52–59.
- [5] Zong, C.; Xu, M.; Xu, L.; Wei, T.; Ma, X.; Zheng, X.; Hu, R.; Ren, B. *Chem. Rev.* **2018**, *118*, 4946–4980.
- [6] Giordano, S.; Morosi, L.; Veglianesi, P.; Licandro, S. A.; Frapolli, R.; Zucchetti, M.; Cappelletti, G.; Falciola, L.; Pifferi, V.; Visentin, S.; D’Incalci M.; Davoli E.; *Sci. Rep.* **2016**, *6* (37027), 1–8.
- [7] Addie, R. D.; Balluff, B.; Bovée, J. V. M. G.; Morreau, H.; McDonnell, L. A. *Anal. Chem.* **2015**, *87* (13), 6426–6433.
- [8] Bocklitz, T. W.; Guo, S.; Ryabchykov, O.; Vogler, N.; Popp, J. *Anal. Chem.* **2016**, *88* (1), 133–151.
- [9] Ozawa, T.; Yoshimura, H.; Kim, S. B. *Anal. Chem.* **2013**, *85* (2), 590–609.
- [10] Sans, M.; Feider, C. L.; Eberlin, L. S. *Curr. Opin. Chem. Biol.* **2018**, *42*, 138–146.
- [11] Chao, Y.; Zhang, T. *Anal. Bioanal. Chem.* **2012**, *404* (5), 1465–1475.
- [12] Ivleva, N. P.; Kubryk, P.; Niessner, R. *Anal. Bioanal. Chem.* **2017**, *409* (18), 4353–4375.
- [13] Ivleva, N. P.; Wagner, M.; Horn, H.; Niessner, R.; Haisch, C. *Anal. Bioanal. Chem.* **2009**, *393* (1), 197–206.
- [14] Taylor, J.; Huefner, A.; Li, L.; Wingfield, J.; Mahajan, S. *Analyst* **2016**, *141*, 5037–5055.
- [15] Ferraro, J. R.; Nakamoto, K.; Brown, C. W. “Chapter 2 - Instrumentation and Experimental Techniques” in “*Introductory Raman Spectroscopy*”, Second Edition; Academic Press, San Diego, **2003**; pp 95–146.
- [16] Enoch, S.; Bonod, N. in “*Plasmonics: From Basics to Advanced Topics*”, Springer-Verlag, Berlin Heidelberg, **2012**.
- [17] Nanophoton Corporation. Raman Spectroscopy, retrieved from www.nanophoton.net. (accessed Dec 4, 2019)
- [18] Wang, Y.; Yan, B.; Chen, L. *Chem. Rev.* **2013**, *113* (3), 1391–1428.
- [19] Masyuko, R.; Lanni, E. J.; Sweedler, V.; Bohn, P. W. *Analyst* **2013**, *138* (7), 1924–1939.
- [20] Sandt, C.; Smith-Palmer, T.; Pink, J.; Brennan, L.; Pink, D. *J. Appl. Microbiol.* **2007**, *103* (5), 1808–1820.
- [21] Allen Institute for Brain Science, Allen Brain Atlas, retrieved from mouse.brain-map.org (accessed Dec 4, 2019)
- [22] Movasaghi, Z.; Rehman, S.; Rehman, I. U. *Applied Spectroscopy Reviews* **2007**, *42* (5), 493–541
- [23] “Nanotechnology Characterization Tools for Biosensing and Medical Diagnosis”; Ed. Kumar, C. S. S. R., Springer-Verlag Berlin Heidelberg, **2018**.
- [24] Tu, Q.; Chang, C. *Biol. Med.* **2012**, *8*, 545–558.
- [25] Andreou, C.; Kishore, S. A.; Kircher, M. F. *J. Nucl. Med.* **2015**, *56* (9), 1295–1299.
- [26] Jamieson, L. E.; Asiala, S. M.; Gracie, K.; Faulds, K.; Graham, D. *Annu. Rev. Anal. Chem.* **2017**, *10*, 415–437.
- [27] Kneipp, J.; Kneipp, H.; Kneipp, K. *Chem. Soc. Rev.* **2008**, *37*, 1052–1060.
- [28] Doering, W. E.; Piotti, M. E.; Natan, M. J.; Griffith Freeman, R. *Adv. Mater.* **2007**, *19*, 3100–3108.
- [29] Haynes, C. L.; Mcfarland, A. D.; Duyne, R. P. Van. *Anal. Chem.* **2005**, *77* (17), 338–346.
- [30] Prochazka, M. in “Surface-Enhanced Raman Spectroscopy - Bioanalytical, Biomolecular and Medical Applications”; Springer International Publishing Switzerland, **2016**.
- [31] Dippel, B. Fundamentals & Technology of Raman Spectroscopy, retrieved from www.raman.de (accessed Dec 4, 2019).
- [32] Lane, L. A.; Qian, X.; Nie, S. *Chem. Rev.* **2015**, *115*, 10489–10529.
- [33] Moskovits, M. *Phys. Chem. Chem. Phys.* **2013**, *15*, 5301–5311.
- [34] Zheng, X.; Jahn, I. J.; Weber, K.; Cialla-May, D.; Popp, J. *Spectrochim. Acta Part A Mol. Biomol. Spectrosc.* **2018**, *197*, 56–77.
- [35] Verdin, A. (Jul 27, 2017) Optimisation de sondes SERS pour des applications bio-analytiques (master’s thesis), Université de Liège, retrieved from MatheO.
- [36] Fabris, L. *J. Opt.* **2015**, *17* (11), 114002.
- [37] Vendrell, M.; Maiti, K. K.; Dhaliwal, K.; Chang, Y. *Trends Biotechnol.* **2013**, *31* (4), 249–257.
- [38] Laing, S.; Gracie, K.; Faulds, K. *Chem. Soc. Rev.* **2016**, *45* (7), 1901–1918.
- [39] Sekula, J.; Niziol, J.; Rode, W.; Ruman, T. *Analyst* **2015**, *140* (18), 6195–6209.
- [40] Chiang, C.-K.; Chen, W.-T.; Chang, H.-T. *Chem. Soc. Rev.* **2011**, *40* (3), 1269–1281.
- [41] Pilolli, R.; Palmisano, F.; Cioffi, N. *Anal. Bioanal. Chem.* **2012**, *402* (2), 601–623.
- [42] Guinan, T.; Kirkbride, P.; Pigou, P. E.; Ronci, M.; Kobus, H.; Voelcker, N. H. *Mass Spectrom. Rev.* **2015**, *34*, 627–640.
- [43] Altuntaş, E.; Schubert, U. S. *Anal. Chim. Acta* **2014**, *808*, 56–69.
- [44] Picca, R. A.; Calvano, C. D.; Cioffi, N.; Palmisano, F. *Nanomaterials* **2017**, *7* (4), 75.
- [45] Arakawa, R.; Kawasaki, H. *Anal. Sci.* **2010**, *26*, 1229–1240.
- [46] Masyuko, R. N.; Lanni, E. J.; Driscoll, C. M.; Shrouf, J. D.; Sweedler, J. V.; Bohn, P. W. *Analyst* **2014**, *139* (22), 5700–5708.
- [47] Aminlashgari, N.; Hakkarainen, M. S. *J. Am. Soc. Mass Spectrom.* **2012**, *23* (6), 1071–1076.
- [48] Lim, A. Y.; Ma, J.; Chiang, Y.; Boey, F. *Adv. Mater.* **2012**, *24*, 4211–4216.
- [49] Phan, N. T. N.; Mohammadi, A. S.; Pour, M. D.; Ewing, A. G. *Anal. Chem.* **2016**, *88*, 1734–1741.
- [50] Song, K.; Cheng, Q. *Appl. Spectrosc. Rev.* **2019**, 1–23.
- [51] Ho, Y.-N.; Shu, L.-J.; Yang, Y.-L. *Wiley Interdiscip. Rev. Syst. Biol. Med.* **2017**, *9* (5), e1387.
- [52] Law, K. P.; Larkin, J. R. *Anal. Bioanal. Chem.* **2011**, *399* (8), 2597–2622.
- [53] Lai, S. K.-M.; Cheng, Y.-H.; Tang, H.-W.; Ng, K.-M. *Phys. Chem. Chem. Phys.* **2017**, *19*, 20795–20807.
- [54] Ng, K.; Chau, S.; Tang, H.; Wei, X.; Lau, K.; Ye, F. *J. Phys. Chem.* **2015**, *119*, 23708–23720.
- [55] Ahlf, D. R.; Masyuko, R. N.; Hummon, A. B.; Bohn, P. W. *Analyst* **2014**, *139*, 4578–4585.